Solar Energy Materials & Solar Cells 148 (2016) 73–86

Contents lists available at ScienceDirect

Solar Energy Materials & Solar Cells

journal homepage: www.elsevier.com/locate/solmat

A computational analysis of coupled thermal and electrical behavior of PV panels

J.C. Sánchez Barroso [a], N. Barth [b], J.P.M. Correia [a], S. Ahzi [a,b,c,*], M.A. Khaleel [b,c]

[a] ICube Laboratory, University of Strasbourg – CNRS, 2 Rue Boussingault, 67000 Strasbourg, France
[b] Qatar Environment and Energy Research Institute (QEERI), HBKU, Qatar Foundation, Doha, Qatar
[c] College of Science and Engineering, HBKU, Qatar Foundation, Doha, Qatar

ARTICLE INFO

Article history:
Received 30 April 2015
Accepted 2 September 2015

Keywords:
Photovoltaic panel
Photovoltaic cell efficiency
Thermal model
Finite difference method

ABSTRACT

In this work, the objective is to develop a simple approach for the prediction of temperature and electrical efficiency of a PV panel. This modeling work constitutes a basic task towards better understanding of the behavior and capabilities of a PV panel when it is subjected to changing meteorological conditions. Different approaches may be used to determine the thermal response of a PV panel depending on the level of details needed for the temperature distribution. For a through-thickness temperature distribution, a one dimensional analysis is necessary. Therefore, only a one-dimensional finite difference model is proposed. Three different formulations of boundary conditions were used and compared in the numerical simulations. To build a full approach for thermal and efficiency analysis, the proposed thermal model is coupled with a solar radiation model and an electrical model. The parameters of the electrical model were estimated by the particle swarm optimization algorithm. Numerical simulations were performed with the meteorological inputs from Ajaccio (France) and for a commercial PV panel BP 350 U. The predictions were compared to existing models and to experimental results.

1. Introduction

Photovoltaic panels (called PV panels in the following) are composed of photovoltaic cells ("PV cells") mounted in series or parallel as modules. They are used to convert the solar energy coming into electrical current. They possess several advantages such as an easy mounting and installation procedure and they do not require sophisticated maintenance. The ability to generate electricity from a natural and vast renewable source makes PV panels a very interesting and promising option to fulfill part of the population's energy consumption, which according to Razykov et al. [1] will be triplicated in about 40 years, up to 30 terawatts in 2050. For such reason, research is a drive forward to improve the efficiency of PV cells. Unfortunately, mass produced PV panels are not yet at perfect conversion rate of the incident solar energy, even though they are more and more an advantageous solution to consider.

In accordance with the work of Armstrong and Hurley [2], the electrical power conversion efficiency for commercial PV modules is currently ranged between 13% and 20%. Consequently, only a small portion of the solar energy absorbed by the PV cells is converted to electricity while the remaining part is converted into heat, which leads to an increase of the PV panel temperature. Skoplaki and Palyvos [3] reported various empirical relations between electrical efficiency and PV panel temperature. From such relations, it can be noticed that an increase of PV panel temperature leads to a decrease of electrical efficiency. Therefore, the PV panel (or PV cell) temperature is a key parameter that must be controlled or decreased in order to achieve a better energy conversion efficiency of the PV cells and thus, a better PV panel performance. However, knowing the manufacturer (data sheet) given cell efficiency is not enough. If the requirement is to know how much energy could be actually obtained from a PV panel, the ambient conditions and the characteristics of the panel should also be taken into account. Therefore, a numerical model capable of integrating the electrical efficiency, the ambient conditions and the panel characteristics is the key to predict, under service conditions, a good estimate of the energy production capabilities of the PV devices.

Several different models were developed to predict the thermal response of a PV panel. A brief summary of different thermal models from the literature is given by Siddiqui et al. [4]. Jones and

* Corresponding author at: Qatar Environment and Energy Research Institute, Qatar Foundation, PO Box 5825, Doha, Qatar. Tel.: +974 4454 1585.
E-mail address: sahzi@qf.org.qa (S. Ahzi).
URLS: http://orcid.org/0000-0002-5519-0513 (N. Barth), http://orcid.org/0000-0002-4881-8392 (J.P.M. Correia), http://orcid.org/0000-0002-0353-9234 (S. Ahzi).

http://dx.doi.org/10.1016/j.solmat.2015.09.004
0927-0248/

Underwood [5] proposed a thermal model for PV panels based on the energy balance equation. In their model, the rate of temperature change is expressed as a sum of convection and radiation heat transfer from the front and rear surfaces of the panel. The thermal model proposed by Jones and Underwood [5] is found to be accurate in clear and overcast conditions. Notton et al. [6] proposed a Finite Difference (FD) model with nodes that represent volumes assumed isothermal. The PV cell temperature is calculated at each node by applying an energy balance equation. With their numerical model, Notton et al. [6] tested various thermal hypotheses found in the literature. The influence of convective transfer coefficients is particularly investigated by Notton et al. [6]. Their numerical predictions are validated using experimental data. Armstrong and Hurley [2] proposed a thermal model that correlates the thermal properties of the PV panel layers with their electrical equivalent by means of a Resistance–Capacitance (RC) circuit. Armstrong and Hurley [2] investigated the influence of varying wind speeds on the PV panel back temperature. Recently, La Brano et al. [7] were able to predict the temperature throughout thickness of the studied device. However, the above mentioned thermal models are only one-dimensional models. A two-dimensional thermal model was developed by Caluianu and Băltăreţu [8] in order to predict the temperature field of PV panel mounted at different distances from a wall. In the numerical work of Caluianu and Băltăreţu [8], the Galerkin Finite Element (FE) approach was used. With this two-dimensional model, the velocity and temperature of air flow between the rear side of PV panel and the wall were predicted. In order to predict the thermal behavior of PV panels with or without cooling, Siddiqui et al. [4] developed a three-dimensional (3D) thermal model using the commercial FE code ANSYS. The effects of changing atmospheric conditions (Middle East climate conditions) and of operating conditions were studied by Siddiqui et al. [4]. Furthermore, they coupled their thermal model with a radiation and an electrical model to predict the thermal and electrical performance of a PV panel with and without a cooling system. Recently, the FE thermal model developed by Siddiqui et al. [4] was sequentially coupled with a structural FE model to predict the performance and the life span of different PV panels (see Hasan and Arif [9]). Most of the numerical studies cited above were focused on calculating the thermal response of a PV panel under varying ambient conditions. In the above-mentioned studies, different assumptions were used to calculate the convective heat transfer coefficients, the radiative heat exchange coefficients and the heat generation inside the panel. The thermal inertia of the panel is usually a key characteristic (Time Constant, see Armstrong and Hurley [2]), it cannot be neglected given the time the panels take to cool down or heat up after any changes in solar irradiance or ambient temperature.

In this work, we propose a coupled approach to predict the thermal and efficiency behavior of PV panels under varying meteorological conditions. In order to predict, in a simple and accurate way, the temperature field inside a PV panel, a one-dimensional (1D) FD thermal model was developed in this work. Accuracy of thermal fluxes is difficult to achieve and thus the definition of thermal boundary conditions is of prime importance – as it was discussed for example by Sartori and Armstrong and Hurley [10,11]. Three different sets of boundary conditions are taken into account in the current work. The sets of boundary conditions are those used by Notton et al. [6], Armstrong and Hurley [2] and by Siddiqui et al. [4]. However, the proposed FD model could be easily adapted to other descriptions of the boundary conditions. The main purpose in this work is to identify, on the thermal response, the influence of different heat exchange assumptions for these three different sets of thermal boundary conditions. Moreover, this modeling is intended to be a first step towards thermal efficiency computation and thermo-mechanical degradation prediction of a PV panel. The FD model can also be later improved towards more realistic thermal simulation of the PV panel, either by taking into account complex thermal environment or by increasing the dimensions of the analysis, as it was both done by Natarajan et al. [12] with 3D FE thermal simulation of complex solar cells.

In addition, the proposed thermal model is sequentially coupled with two additional models to form a multi-physics model capable of predicting the thermal and electrical response of a PV panel. The first additional model used to determine the amount of solar energy absorbed by the PV panel and is known as the radiation model. The second additional model is used to predict the *I–V* curve at a specific operating point and it is known as the electrical model. In this work, the electrical model is based on the well-known one-diode electrical analogy (based on the expressions given by Siddiqui et al. [4] and Tsai [13]). The required electrical parameters are calculated using a developed optimization method based on the movement of swarms [14]. A complete description of the models implemented in this study is given in the following section.

2. Multi-physics modeling of PV panels

A multi-physics model is proposed in this work to study the thermal response of a PV panel while it works under continuously changing ambient conditions. The model sequentially couples a solar radiation model that calculates the amount of solar energy absorbed by the PV cells, a thermal model that calculates the heat fluxes inside the PV panel and the heat interactions with the surroundings and, finally, an electrical model capable of determining the electrical performance of the panel at a given operating point.

2.1. Solar radiation model

The objective of the solar radiation model is to calculate the amount of solar radiation absorbed by the PV cells. This determines in turn the amount of energy available for electrical conversion in the cells. The main input is the measured solar radiation flux, taking into account its direct beam and diffuse components. The model selected for this study is used in the work of Notton et al. [6], based on the ASHRAE convention. The absorbed solar radiation S is estimated by the equation [15]:

$$S = (\tau_{fg}\alpha_{PV})_n \left[R_b G_b K_b + G_d K_d \frac{1+\cos\beta}{2} + (G_b + G_d)\rho_{ground} K_{ground} \frac{1-\cos\beta}{2} \right] \quad (1)$$

where $(\tau_{fg}\alpha_{PV})_n$ is the normal transmitivity – absorptivity product (the term "normal" represents a zero incidence angle), R_b is the ratio of beam radiation on tilted plane to beam radiation on horizontal plane, G_b the beam solar radiation flux on a horizontal plane, G_d the diffuse solar radiation flux on a horizontal plane, K is the incidence angle modifier for the beam, diffuse and ground-reflected radiations, ρ_{ground} the reflectivity of the ground (also called albedo) and β is the tilt angle of the panel (see the schematic representing the panel in Fig. 1). The ratio of beam radiation on the tilted plane to that on the horizontal plane R_b is calculated as follows:

$$R_b = \frac{\sin(\alpha+\beta)}{\sin(\alpha)} \quad (2)$$

where α is the elevation angle and β is the tilt angle of the PV panel (see Fig. 1). The elevation angle α is calculated with the

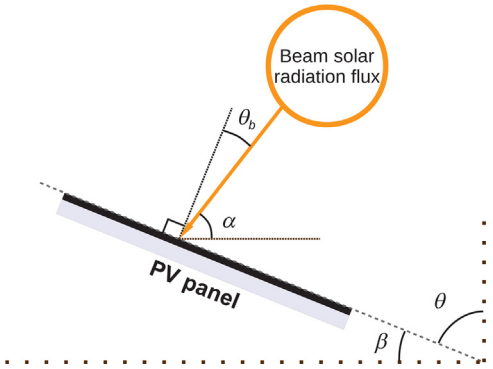

Fig. 1. Definition of the different angles of a PV panel.

following equation:

$$\alpha = 90 - \varphi + \delta \tag{3}$$

and the declination δ is given as follows:

$$\delta = 23.45 \ \sin\left[\frac{360}{365}(284+d)\right] \tag{4}$$

Here φ is the latitude of the location where the PV panel is placed and d is the day of the year. In accordance with the work of Notton et al. [6], the incidence angle modifier of the direct component of solar radiation is given by:

$$K_b = 1 + b_0\left(\frac{1}{\cos\theta_b} - 1\right) \tag{5}$$

where θ_b is the incidence angle of the beam solar radiation and the constant b_0 is taken equal to -0.1, as proposed in Notton et al. [6]. The incidence angle modifiers for the diffuse and ground-reflected radiations are given by the following expressions:

$$K_d = 1 + b_0\left(\frac{1}{\cos\theta_d} - 1\right) \tag{6}$$

$$K_{ground} = 1 + b_0\left(\frac{1}{\cos\theta_{ground}} - 1\right) \tag{7}$$

where θ_d and θ_{ground} are respectively the incidence angles for the diffuse and ground-reflected radiations. Their expressions are given, according to Duffie and Beckman [15], as a function of the tilt angle β of the PV panel:

$$\theta_d = 59.68 - 0.1388\beta + 0.001497\beta^2 \tag{8}$$

$$\theta_{ground} = 90 - 0.5788\beta + 0.002693\beta^2 \tag{9}$$

The incidence angle of the beam solar radiation is calculated with the expression (see Fig. 1):

$$\theta_b = 90 - (\beta + \alpha) \tag{10}$$

2.2. Thermal model

2.2.1. Governing equations

The thermal model presented below was developed to predict the temperature field throughout the PV panel thickness. The studied PV panel is a commercial PV panel BP350U. Given the reduced thickness of the panel in comparison with its length and width, thermal exchanges from the sides of the PV panel are assumed to be negligible. Thus, it is possible to consider the PV panel as a one-dimensional domain. The domain is extended in the direction normal to the greatest area of the PV panel.

The basic equation of the thermal model is the heat transfer equation for a solid domain given by:

$$\rho c_p \frac{\partial T}{\partial t} = \nabla \cdot k\nabla T + Q \tag{11}$$

where ρ is the density, c_p is the specific heat capacity at constant pressure, and k is the thermal conductivity of the considered material. This is a partial differential equation derived by time t on the left and in the right term by space, i.e. x, through the gradient operator. Q is the internal heat source at the point or location of interest. In Eq. (11), it is important to note that material properties such as the density ρ or the specific heat capacity c_p change according to the location (i.e. materials encountered along the thickness of the PV panel). To complete the thermal model, boundary conditions must be defined for Eq. (11), namely the internal heat fluxes or thermal fluxes produced by convection or radiation of the panel surfaces with the environment.

2.2.2. Thermal load and boundary conditions

The internal heat flux Q in Eq. (11) comes from the part of the incident solar power that is not converted to electricity, raising the temperature of the PV panel. The expression to calculate such flux is taken from the work of Siddiqui et al. [4] and it is given by:

$$Q = \frac{S \times A_{PV,panel}}{V_{PV,cells}}(1 - \eta_{PV}) \tag{12}$$

where $A_{PV,panel}$ is the area of the PV panel covered by PV cells, $V_{PV,cells}$ the volume of the PV cells inside the PV panel and η_{PV} is the electrical power efficiency coefficient of the PV cells which can be defined as function of temperature following the linear expression [3]:

$$\eta_{PV} = \eta_{PV,Tref}\left[1 - \beta_{ref}(T_{PV} - T_{PV,ref})\right] \tag{13}$$

where $\eta_{PV,Tref}$ is the electrical efficiency at reference temperature, β_{ref} is a temperature coefficient, T_{PV} is the temperature of the PV cells and $T_{PV,ref}$ is the reference temperature. The parameters $\eta_{PV,Tref}$ and β_{ref} depend mainly on the type of the PV cells used in the module. In accordance with the work of Notton et al. [6], the proposed thermal model also takes into account the heat generated in the front glass of the PV panel, expressed by:

$$Q_{fg} = \frac{\alpha_{fg} \times G \times A_{PV,panel}}{V_{fg}} \tag{14}$$

where α_{fg} is the absorptivity coefficient of the glass, G is the measured global solar radiation flux and V_{fg} is the volume of the glass.

Since the proposed thermal model takes into account different environmental conditions (solar radiation flux, ambient temperature, wind speed, etc.), the heat exchanges with the thermal environment must be expressed with care. These thermal boundary conditions can be described in terms of two different physical phenomena, convection and radiation. The convection with the air is expressed by:

$$q_{conv} = h_{conv}(T_S - T_{amb}) \tag{15}$$

and the radiation with the sky or ground, expressed by:

$$q_{rad} = \varepsilon \times \sigma\left(T_S^4 - T_0^4\right) \tag{16}$$

In Eq. (15), h_{conv} is the film coefficient for the convection from the surface which is at the temperature T_S, this convection being done by the air at the temperature T_{amb}. It should be noted that h_{conv} can be stated differently for free convection and forced convection. In Eq. (16), ε is the emissivity of the surface, σ is the Stefan–Boltzmann constant and T_0 is the sink temperature. It should be noted that the expression of Eq. (16) can be further developed with different view factors, depending on the solid

angles assumed for this radiant surface with the different black bodies at their own different sink temperature (two different ones in our study: the sky or the ground).

Convection boundary conditions are applied following different formulations to the front and rear surfaces of the PV panel. These boundary conditions are defined via the equivalent heat exchange coefficient h_{conv}. Three different formulations (proposed in the works of Notton et al. [6], Armstrong and Hurley [2] and Siddiqui et al. [4]) are considered to calculate the convection heat exchange coefficient. The differences between these works are not only the equations used but also the assumptions regarding the use of the free and forced coefficients in the front and rear surfaces of the PV panel.

In the work of Notton et al. [6], a large study was conducted to determine the best possible formulation to calculate the convection heat exchange coefficient. In their work, Notton et al. [6] concluded that the best option is to consider only the forced convection for both sides of the PV panel, and used the expression proposed by Cole and Sturrock [16]:

$$h_{conv,forced} = 11.4 + 5.7w \tag{17}$$

where w is the wind speed. However, in the work of Armstrong and Hurley [2], forced convection is applied only on the front surface of the PV panel (for the rear surface, $h_{rear} = h_{conv,free}$, see below). The relation used by Armstrong and Hurley [2] to express the forced convection coefficient is the one proposed by Test et al. [17]:

$$h_{conv,forced} = 8.55 + 2.56w \tag{18}$$

The front and rear surfaces of the PV panel are also submitted to free convection in the work of Armstrong and Hurley [2]. For both surfaces, the free convection coefficient is calculated with a specific expression of the Nusselt number, using the following relation:

$$h_{conv,free} = \frac{Nu \times k_{air}}{L_{PV,panel}} \tag{19}$$

where Nu is the Nusselt number, k_{air} is the thermal conductivity of the air and $L_{PV,panel}$ is the characteristic length of the PV panel. In this study, the characteristic length taken is the longest dimension of the PV panel given in the datasheet provided by the manufacturer. The wind is then assumed to travel in the direction corresponding to such length, resulting in a constant $L_{PV,panel}$ through all the simulation. For the front side of the panel, Armstrong and Hurley [2] used the Nusselt number expression defined by Bejan and Kraus [18]:

$$Nu = 0.14\left[(Gr \times Pr)^{1/3} - (Gr_{cr\times} Pr)^{1/3}\right] + 0.56\left(Gr_{cr} \times Pr \times \cos\theta\right)^{1/4} \tag{20}$$

where Gr is the Grashof number, Pr is the Prandtl number, Gr_{cr} is the critical Grashof number and θ is the angle of inclination of the PV panel with the vertical. In the case of the bottom surface, Armstrong and Hurley [2] used the Nusselt number expression given by Incropera and DeWitt [19]:

$$Nu = \left[0.825 + \frac{0.387 \times Ra^{1/6}}{\left[1 + (0.492/Pr)^{9/16}\right]^{8/27}}\right]^2 \tag{21}$$

where Ra is the Rayleigh number.

Since Armstrong and Hurley [2] assumed that the front surface of the panel is also submitted to both free and forced convective hear exchanges, an effective convection heat transfer coefficient for the front surface must be calculated. In Armstrong and Hurley [2], the film effective coefficient, for the front surface only, is then given by the following expression [19]:

$$h_{front} = h_{conv} = \sqrt[3]{h_{conv,forced}^3 + h_{conv,free}^3} \tag{22}$$

Recently, in the thermal model of Siddiqui et al. [4], the forced and free convection heat exchange were assumed to happen on both surfaces of the PV panel. Siddiqui et al. [4] used the relations proposed by Sparrow et al. [20] and by Lloyd and Moran [21] to respectively calculate the forced and free convection coefficients. The forced convective heat exchange coefficient is given by:

$$Nu = 0.86 \times Re^{1/2} \times Pr^{1/3} \tag{23}$$

where Re is the Reynolds number. The free convective heat exchange coefficient, derived from the Nusselt number given by Lloyd and Moran [21], is expressed by:

$$Nu = \left\{ \begin{array}{c} 0.76 \times Ra^{1/4} \ \text{ for } \ 10^4 < Ra < 10^7 \\ 0.15 \times Ra^{1/3} \ \text{ for } \ 10^7 < Ra < 3 \times 10^{10} \end{array} \right\} \tag{24}$$

The different convection heat exchange coefficients (forced or free) are calculated from the Nusselt number using Eq. (19). In the work of Siddiqui et al. [4], both coefficients are summed directly to form an equivalent convection heat exchange coefficient.

The radiation heat exchange is accounted for in the thermal model through a radiation coefficient which, in general terms, is defined in the same way by Notton et al. [6] and Armstrong and Hurley [2]. The radiation heat exchanges are calculated in the thermal model using Eq. (16). In all the considered studies [2,4,6], the radiation exchanges of the front and rear surfaces to the sky or ground are taken into account and differentiated by the use of a geometric factor. The expression to calculate the radiation heat loss coefficient is then defined by:

$$q_{rad} = \varepsilon_{front/rear} \times F_{front/rear-sky/ground} \times \sigma\left(T_{front/rear}^4 - T_{sky/ground}^4\right) \tag{25}$$

where ε_{front} is the emissivity of front surface of the PV panel, ε_{rear} is the emissivity of the rear surface, F are geometric factors for radiation of the front or rear surfaces to sky or ground, T_{front} is the temperature of the front surface, T_{rear} is the temperature of the rear surface, T_{sky} is the sky temperature and T_{ground} is the ground temperature. On the contrary, Siddiqui et al. [4] used the expression proposed by Duffie and Beckman [15] to define the radiation coefficient, which includes the emissivity of the ground, given by:

$$q_{rad} = \varepsilon_{front/rear} \times F_{front/rear-sky} \times \sigma\left(T_{front/rear}^4 - T_{sky}^4\right) + \frac{F_{front/rear-ground} \times \sigma\left(T_{front/rear}^4 - T_{ground}^4\right)}{\frac{1}{\varepsilon_{front/rear}} + \frac{1}{\varepsilon_{ground}} - 1} \tag{26}$$

It should be noticed that if the emissivity of the ground, ε_{ground}, is equal to 1, Eq. (26) changes to the form given in Eq. (25). The different geometric factors F in Eqs. (25) and (26) are functions of the PV panel inclination β and can be found in the work of Armstrong and Hurley [2].

Furthermore, the sky and ground temperatures must be estimated since they are required in Eqs. (25) and (26). The sky temperature is another parameter calculated differently in the three different thermal models considered in the present work. In the work of Notton et al. [6] the expression given by Swinbank [22] is used and is given by:

$$T_{sky} = 0.0552 \times T_{amb}^{1.5} \tag{27}$$

Armstrong and Hurley [2] did not specify the expression used to calculate the sky temperature. Therefore, we assumed it to be equal to the ambient temperature (i.e. with cloudy sky conditions). In the work of Siddiqui et al. [4] the sky temperature is defined

with the equation given by Jones and Underwood [5]:

$$T_{sky} = T_{amp} - \delta T \quad \text{with} \quad \delta T = 20\ \text{K} \ \text{(in clear sky conditions)} \tag{28}$$

Contrary to sky temperature estimation, the ground temperature was simply assumed equal to the ambient temperature in all the considered studies [2,4,6].

2.2.3. Thermal model implementation

A finite difference (FD) approach is used to numerically solve the heat transfer equation, Eq. (11). To develop a one-dimensional FD scheme, a grid must first be constructed. To do so the thickness of the PV panel is subdivided into N equally spaced points. A grid point, also called node, can be defined by its coordinate:

$$x_i = i\Delta x \ \text{ with } \ 1 \le i \le N \tag{29}$$

where $\Delta x = t_{PV,panel}/N$ is the thickness increment. The first node of the model ($i=1$) is located at the bottom or rear surface of PV panel (i.e. $x=0$), while the last node ($i=N$) is located at the front or top surface (i.e. $x=t_{PV,panel}$). Taking into account the spatial discretization of the problem, the spatial derivatives are approximated by a first-order central finite difference scheme as follows:

$$\frac{\partial Y(x)}{\partial x} \approx \frac{Y_{i+1} - Y_{i-1}}{2\Delta x} \tag{30}$$

For the time derivative there are several possibilities to express in terms of FD approximation. In this work, we have decided to use a backward difference scheme given by:

$$\frac{\partial}{\partial t}T(x,t) \approx \frac{T(x,t+\Delta t) - T(x,t)}{\Delta t} = \frac{T_i^{n+1} - T_i^n}{\Delta t} \tag{31}$$

where Δt is the time increment. With the help of Eqs. (30) and (31), the heat transfer equation, Eq. (11), is discretized as follows:

$$\rho_i c_{p,i} \frac{T_i^{n+1} - T_i^n}{\Delta t} = \frac{1}{\Delta x}\left[k_{i+1/2}\left(\frac{T_{i+1}^{n+1} - T_i^{n+1}}{\Delta x}\right) - k_{i-1/2}\left(\frac{T_i^{n+1} - T_{i-1}^{n+1}}{\Delta x}\right)\right] + Q_i \tag{32}$$

The present FD model has an implicit time scheme, making the model unconditionally stable. It should be noticed that the expression of Eq. (32) is valid only for the internal nodes of the domain (i.e. $i=2, 3, \ldots, N-1$).

For the nodes at the boundaries it is required to include the equivalent heat exchange coefficient, h, which includes the convection and radiation heat exchange coefficients. The discretized heat transfer equations for the nodes located at the boundaries of the domain are obtained from an energy balance of half of the volume formed between the boundary node and the node adjacent to it. The equation of the energy balance for the rear surface of the PV panel (i.e. $i=1$) is:

$$\rho_1 A_{panel}\frac{\Delta x}{2} c_{p,1}\frac{T_1^{n+1} - T_1^n}{\Delta t} = kA_{panel}\left(\frac{T_2^{n+1} - T_1^{n+1}}{\Delta x}\right) + hA_{panel}\left(T_{amb}^{n+1} - T_1^{n+1}\right) + Q_1 A_{panel}\frac{\Delta x}{2} \tag{33}$$

while the equation of the energy balance for the front surface of the PV panel (i.e. $i=N$) is:

$$\rho_N A_{panel}\frac{\Delta x}{2} c_{p,N}\frac{T_N^{n+1} - T_N^n}{\Delta t} = kA_{panel}\left(\frac{T_{N-1}^{n+1} - T_N^{n+1}}{\Delta x}\right) + hA_{panel}\left(T_{amb}^{n+1} - T_N^{n+1}\right) + Q_N A_{panel}\frac{\Delta x}{2} \tag{34}$$

where A_{panel} is the area of the PV panel covered by PV cells. Rearranging Eqs. (33) and (34) yields:

$$\begin{cases} \rho_1 c_{p,1}\frac{T_1^{n+1} - T_1^n}{2\Delta t} = k\left(\frac{T_2^{n+1} - T_1^{n+1}}{\Delta x^2}\right) + hA_{panel}\left(\frac{T_{amb}^{n+1} - T_1^{n+1}}{\Delta x}\right) + \frac{Q_1}{2} \\ \rho_N c_{p,N}\frac{T_N^{n+1} - T_N^n}{2\Delta t} = k\left(\frac{T_{N-1}^{n+1} - T_N^{n+1}}{\Delta x^2}\right) + hA_{panel}\left(\frac{T_{amb}^{n+1} - T_N^{n+1}}{\Delta x}\right) + \frac{Q_N^1}{2} \end{cases} \tag{35}$$

The general system formed by Eqs. (32) and (35) is classically arranged in a way that all the known terms are kept at the right hand side of the system, keeping the unknown parameters at the left hand side, leading to a system of linear equations. In the present work, the system of linear equations is solved in MATLAB® environment for every time step. Then, at each time the temperatures of the previous step are updated with the ones obtained in the current step.

2.3. Electrical model

In a PV panel, the PV cells are mounted in arrays connected in series and/or parallel to produce the desired output voltage, current or power. The one-diode model, coming from an electrical analogy of the PV cells, can be used to describe the electrical behavior of a PV panel. In this work two modified one-diode models are studied, the first is presented by Siddiqui et al. [4] and the second one was used by Tsai [13].

Based on the one-diode model, the current and voltage relationship (or I–V characteristic) at a fixed cell temperature and solar radiation for the equivalent circuit proposed by Siddiqui et al. [4] is expressed by:

$$I = I_L - I_0\left(\exp\left(\frac{V + IR_s}{a}\right) - 1\right) - \frac{V + IR_s}{R_{sh}} \tag{36}$$

where I is the current and V is the voltage/potential at the terminals of the circuit, I_L is the current source (also called photocurrent), I_0 is the diode reverse saturation current, R_s is the series resistance and R_{sh} is the shunt resistance and a a modified diode ideality factor given by the following relation:

$$a = \frac{N_s k_B A T_{PV}}{q_e} \tag{37}$$

where N_s is the number of PV cells connected in series, k_B is the Boltzmann constant, A is the diode ideality factor, T_{PV} is the temperature of the PV cells and the constant q_e is the electron charge. In the expression given in Eq. (37) only the cells connected in series in a PV panel are taken into account. However, the electrical model proposed by Siddiqui et al. [4] can also be applied for PV panels with strings of cells connected in parallel. In agreement with Alsayid [23], the currents I_0 and I_L and the resistances R_s and R_{sh} in Eq. (36) can be rewritten in order to take into account the number of cells arranged in parallel.

In the work of Tsai [13], the electrical model is governed by the following expression:

$$I = N_p I_L - N_p I_0\left(\exp\left(\frac{q_e}{k_B A T_{PV}}\left(\frac{V}{N_s} + \frac{IR_s}{N_p}\right)\right) - 1\right) - \frac{(N_p/N_s)V + IR_s}{R_{sh}} \tag{38}$$

where N_p is the number of cells connected in parallel and N_s is the number of cells connected in series inside the PV panel. In this work, both models are used to obtain the I–V curves for a commercial PV panel BP 350 U. It should be noted that for this device $N_p=2$ and $N_s=36$. In order to use Eqs. (36) and (38), electrical parameters like the diode reverse saturation current, I_0, and the series and shunt resistances, R_s and R_{sh}, must be estimated before, since they are not usually provided by the PV manufacturer. The optimization method of the parameters included in Eq. (38) is presented in the work of Tsai [13] and relies on an incremental search. However, in the current work, a more general method

Table 1
Characteristics of the layers constituting the PV panel BP 350, from Armstrong and Hurley [2].

Layer	Thickness [$\times 10^{-3}$ m]	Thermal conductivity k [W/m/K]	Density ρ [kg/m^3]	Specific heat capacity c_p [J/kg/K]
1. Glass (front)	3	1.8	3000	500
2. ARC	0.0001	32	2400	691
3. PV cells	0.225	148	2330	677
4. EVA	0.5	0.35	960	2090
5. Rear contact	0.01	237	2700	900
6. Tedlar (rear)	0.1	0.2	1200	1250

capable of determining the parameters for the one-diode model was also used. This method is based on the Particle Swarm Optimization (PSO) algorithm is presented in the work of Sánchez Barroso et al. [14].

3. Thermal model validation

As mentioned before, the main objective of the model is to determine the temperatures in each one of the layers of the PV panel, taking into account the thermal response in time. In order to verify the validity of our 1D FD model, implemented in MATLAB® 7.10.0, a preliminary calculation was performed and compared with the experimental results of Armstrong and Hurley [2], where the PV panel is BP 350 which has 72 multicrystalline Si cells ($N_p=2$, $N_s=36$). The material properties of each component of the PV panel layers are given in Table 1. The information was obtained from the BP Solar website, the STR Photocap Solar Cell Encapsulants website, Matsukawa and Kurokawa [24], Lu and Yao [25], Jones and Underwood [5], Notton et al. [6], Jooß [26], Lai et al. [27], Phylipsen and Alsema [28] and Hatsch [29]. The thin film area for all the layers is assumed to be the area covered by the 72 PV cells in the PV panel. Areas of the module without PV cells are not considered.

In order to reduce computational costs, additional assumptions were defined:

- All the material properties of the different layers in the PV panel are assumed to be isotropic and temperature independent.
- The ambient temperature is assumed to be equal in all sides of the PV panel.
- The ARC and Rear contact layers are neglected.

This last assumption is due to the fact that their thicknesses are very small compared to the other layers, and they are not expected to be noteworthy thermal resistances due to the magnitude of their thermal properties detailed in Table 1. Consequently, only four layers of the PV panel are taken into account (front Glass, PV Cell, EVA and Tedlar).

Armstrong and Hurley [2] measured, during 35 min, the real operating conditions of the PV panel subjected to a wind speed of 0.77 m/s and defined the following boundary conditions: forced convection coefficient (10.53 W/m^2/K) and free convection coefficient (5.81 W/m^2/K). The following additional assumptions are used for our simulations:

- Initial PV panel temperature of 288.15 K (15 °C)
- Constant ambient temperature of 288.15 K (15 °C)
- Ground and sky temperatures equal to the ambient temperature
- Absorbed solar radiation is equal to the measured solar radiation
- Zero tilt angle ($\beta=0°$)
- Electrical efficiency of 13.4%
- PV cell temperature coefficient $\beta_{ref}=0.5\%/°C$

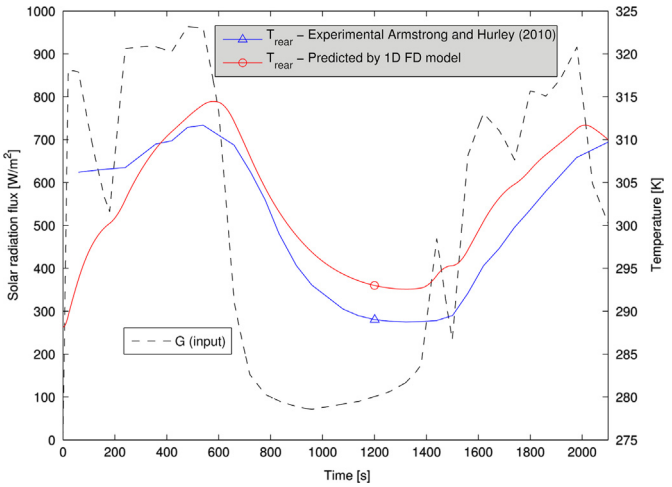

Fig. 2. Thermal response at the rear contact of the PV panel with a fixed wind speed of 0.77 m/s according to Armstrong and Hurley [2] and the implemented 1D FD model. (For interpretation of the references to color in this figure, the reader is referred to the web version of this article.)

Furthermore, the normal transmitivity of the front glass τ_{fg} and the normal absorptivity of the PV cell α_{PV} are taken from the work of Notton et al. [6], with the values of 0.95 and 0.9 respectively. The absorptivity of the front glass α_{fg} is also taken from the same work with a value of 0.05. All these values have been provided by Photowatt and can be found in the work of Notton et al. [6]. The emissivity of the front glass surface ε_{front} and the rear surface ε_{rear} are assumed as 0.91 and 0.85 respectively, taken from Notton et al. [6] and Morgan et al. [30]. These values have been used by Armstrong and Hurley [2] for the panel BP 350 U.

The FD simulation was performed with 154 nodes equally spaced through the PV panel thickness (spatial discretization $\Delta x=25\times10^{-6}$ m) and with a time discretization $\Delta t=0.01$ s. In Fig. 2, the dashed line is the measured global radiation digitized from Armstrong and Hurley [2] and used as direct input for FD simulations. The FD predictions are also reported in Fig. 2.

In Fig. 2, solid lines are numerical (red with circle symbol) and experimental (blue with triangle symbol) results for the temperature of the rear surface. The temperature response predicted with the FD model is close to the experimentally measured one by Armstrong and Hurley [2]. In general, both curves have a similar behavior, differentiated by less than 5 degrees in most of the simulation time. The discrepancy between the FD prediction and Armstrong and Hurley [2] observations could be due to the differences between modeled thermal fluxes and experimental ones, but a particular tolerance should be kept in mind for the initial state of the PV cell (defined in the model at the ambient temperature instead of the initial experimental temperature). However, the observed differences can be considered acceptable given the assumptions made and due to the lack of real-time information.

The proposed 1D FD model was also validated by means of a comparison with a 2D FE model that was developed using the commercial code ABAQUS [31]. The protocol applied in this FE modeling is the same as in Barth et al. [32]. But instead of a 3D model a 2D design representing the PV panel was used. The designed 2D plane contains the normal vector to the PV panel

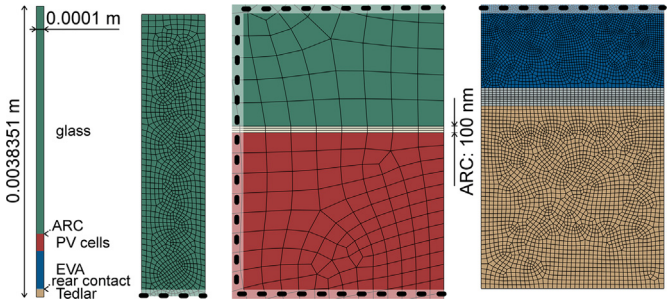

Fig. 3. 2D mesh design of the BP 350 U solar cell for the FE model [33]. The vertical axis coincides with the normal vector to the PV panel surface. The 6 layers, represented by different colors, are from the front (up) to the rear side of the panel: glass, ARC, PV cells, EVA, rear contact and Tedlar (see Table 1 for their thickness). Dashed lines are the discontinuities in various zooms from the global geometry (this latter is on the left, without the designed elements). (For interpretation of the references to color in this figure legend, the reader is referred to the web version of this article.)

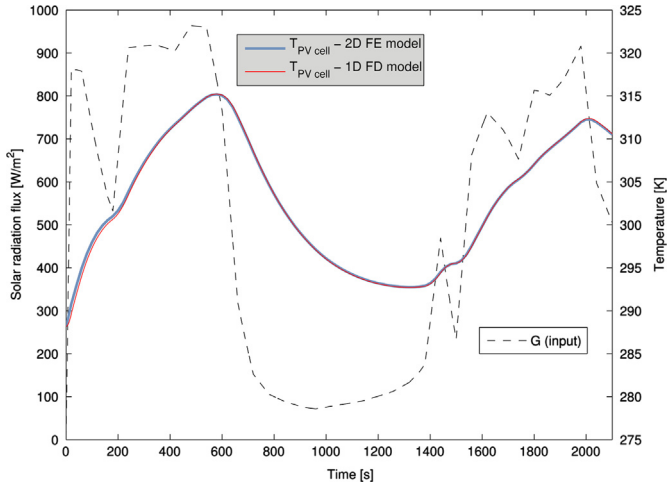

Fig. 4. Comparison of the PV cell temperature obtained with the 1D FD model and the 2D FE model using the input data presented in the work of Armstrong and Hurley [2] (the case of wind speed equal to 0.77 m/s).

plane, with an arbitrary width of 10^{-4} m. The electron collecting grid over the glass at the front surface was not taken into account. In this way, the symmetries applied on the design allow us also to model a panel without border effects. This FE model is then designed to study the evolution of the transient temperature field as a function of the depth along the section, and consequently the thermal response of the PV cell can be computed. 158,000 linear quadrilateral elements (DC2D4 type) were used in this 2D FE model, with various mesh refinements to enable the correct modeling of the thin films piled inside the cell (Fig. 3 represents some of these mesh features). The mesh has a total of 160,000 degrees of freedom (this is also the number of its nodes).

In this FE thermal model, the thermal properties for conduction are those found in Table 1. The thermal fluxes described in the work of Armstrong and Hurley [2] were used for the FE simulations. The solar power inputs and the thermal fluxes were mainly scripted into the FORTRAN 77 user subroutines HETVAL, DFLUX, FILM of ABAQUS [31]. DFLUX introduce the solar power directly on the ARC/PV cells interface, and this incident thermal source is compensated (in HETVAL) by a thermal volume flux Q which is constant over the whole layer of the PV cells. In this way, we take into account, with Q, the efficiency of the solar cell as a function of its temperature, using the classical power efficiency coefficient dependence of Eq. (13). The same boundary conditions, defined in Armstrong and Hurley [2], were used for both the 2D FE model as well as the 1D FD model. In both models, the initial temperature was taken equal to 288.15 K (15 °C) in the whole PV panel, for the sake of clarity and reproducibility of our studies here.

The FE predictions are presented in Fig. 4. No difference between the predictions of the 1D FD model and the 2D FE model can be observed, even for the temperature jump at 0 s (this T-jump induced by solar irradiance is only due to the assumption that the initial temperature of the PV cell models is equal to the ambient temperature, which is lower than the initial experimental temperature). Both models provide the same results even with the different layers taken into account (ARC and rear contact are neglected in the 1D FD model). The results show that a simplified model such as the one implemented with the 1D FD model, or the 2D FEM model, can predict the PV cell temperature with a fair agreement to the experimental results. These results also show that ARC and rear contact are not significant thermal resistances in the thickness of a BP350 U PV module.

4. Results and discussion

4.1. Comparison of the three thermal boundary conditions

As mentioned before, one of the objectives of this work is to compare the assumptions used in the formulations of existing approaches and observe the different results they may provide. Such comparison is presented in this section. The first result to be analyzed is the PV cell temperature while using the Nominal Operating Cell Temperature (NOCT) conditions. The NOCT is routinely provided by PV manufacturers in their datasheets. According to the module datasheet, the panel BP 350U has a NOCT of 47 ± 2 °C. For each one of the three sets of thermal boundary conditions used, the temperatures of the PV cells were computed with the proposed 1D FD model at NOCT conditions. These temperatures are reported in Table 2 after a 35-min transient period (equilibrium is reached at a time near of 10 min from the initial T at T_{amb}). The numerical results given in Table 2 show important differences between the three cases (5.7 °C standard deviation). The assumptions proposed by Armstrong and Hurley [2] give the highest temperature and the closest one to the NOCT found in the datasheet, with just a difference of half degree. The formulations proposed by Notton et al. [6] underestimate the temperature by almost 12 °C with respect to the reference and, finally, the formulations of Siddiqui et al. [4] underestimate the NOCT by nearly 7 °C.

Running the thermal model with NOCT conditions offers a general overview of the model behavior. On a more general context, it is required to run the model using real meteorological data in order to have a better exploration of effects for the different formulations. Professor G. Notton provided us with all the required data measured in a laboratory located in Ajaccio, France. Such data are used in this study to analyze the different sets of thermal boundary conditions chosen from the literature. The analysis starts with 30 min of data corresponding to the first day of July of 2002, at noontime. The experimental data were recorded in a minute-

Table 2
Final PV cell temperatures predicted at NOCT conditions.

Thermal model assumptions	1D FD model NOCT [in °C]	Relative error [°C]
Notton et al. [6]	35.05	−12
Armstrong and Hurley [2]	46.45	−0.5
Siddiqui et al. [4]	39.95	−7

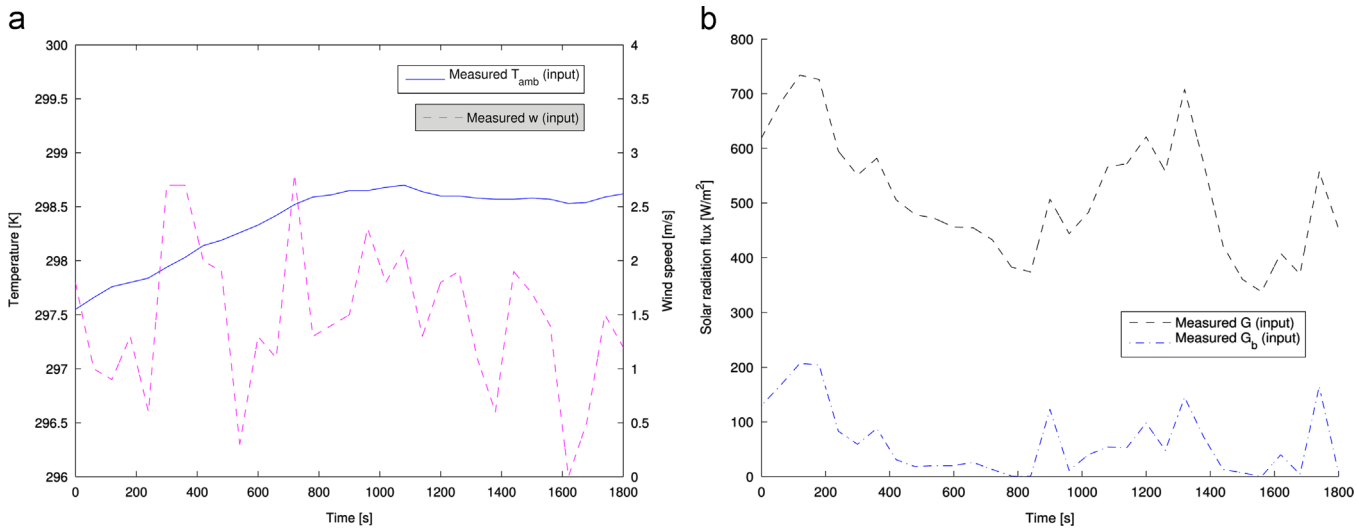

Fig. 5. Model inputs from Ajaccio corresponding to the 1st of July or 2002, at noontime: (a) measured ambient temperature and wind speed and (b) measured global and beam solar radiations.

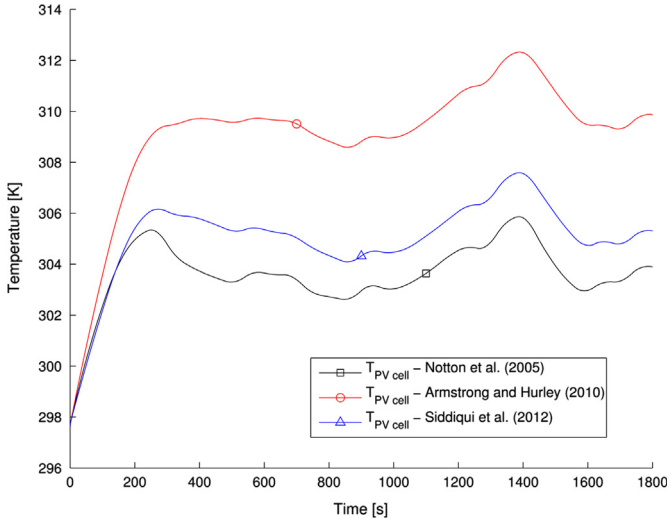

Fig. 6. PV cell temperatures predicted by the 1D FD model using the formulations of the considered three thermal boundary conditions.

by-minute basis and it is considered sufficient to observe differences between the sets of boundary conditions used. The experimental data provided by Professor G. Notton and recorded in such period of time are shown in Fig. 5.

In Fig. 5 it can be observed that three out of the four main inputs have important variations over what could be considered as a small period of time, taking into account that meteorological data of even one year could be studied. The PV cell temperatures predicted by the FD model with the three sets of boundary conditions are plotted in Fig. 6.

The first thing to notice in Fig. 6 is that the tendency observed in the NOCT evaluation is also maintained here. The boundary conditions applied in Armstrong and Hurley [2] result in a higher temperature of the PV cell in comparison with the other two cases. The boundary conditions used by Notton et al. [6] give again the lower temperatures. Even though the curves follow similar trend, the temperature response of the panel is different depending on the considered assumptions. In the case of the boundary conditions of Armstrong and Hurley [2], the temperature curve is immediately nearly flat after the initial temperature increase, even when the changes in the measured global radiation are important, which means the model responds slowly with respect to the

Table 3
Cases investigated in the parametric study on PV cell temperatures.

Case	Ambient temperature T_{amb} [K]	Global solar radiation flux G [W/m^2]	Beam solar radiation flux G_b [W/m^2]	Wind speed w [m/s]
1	288.15–308.15	600	100	1
2	298.15	400–800	100	1
3	298.15	600	0–200	1
4	298.15	600	100	0–4

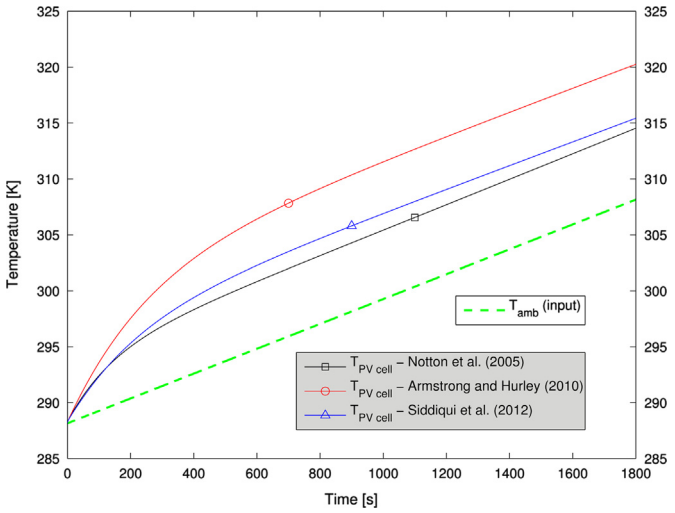

Fig. 7. PV cell temperatures with changing ambient temperature.

variations of meteorological data. In the other two cases the temperature fluctuates a little more, showing a slightly quicker response.

These variations are due to the relative fluctuations and importance of solar irradiance, wind speed and ambient temperature and their influences on the energy balance, i.e. influence of heat and cooling through the different thermal boundary conditions. To moderate the influence of such complex variations on the energy balance, a different approach is now proposed to evaluate the response of the FD model, in which only one of four main inputs is varied while the others are kept constant. Such

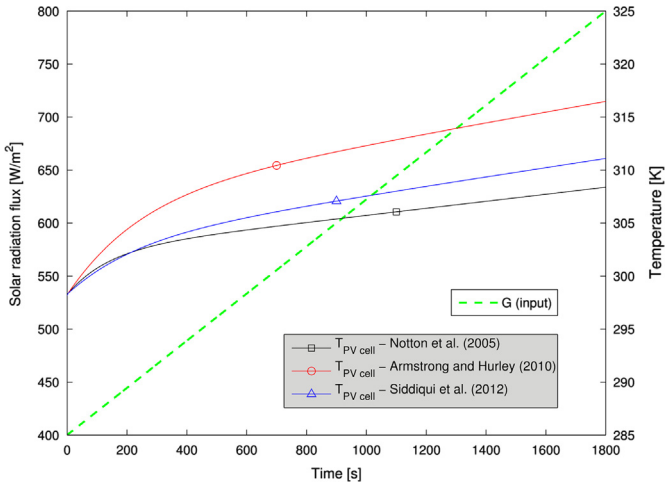

Fig. 8. PV cell temperatures with changing global solar radiation.

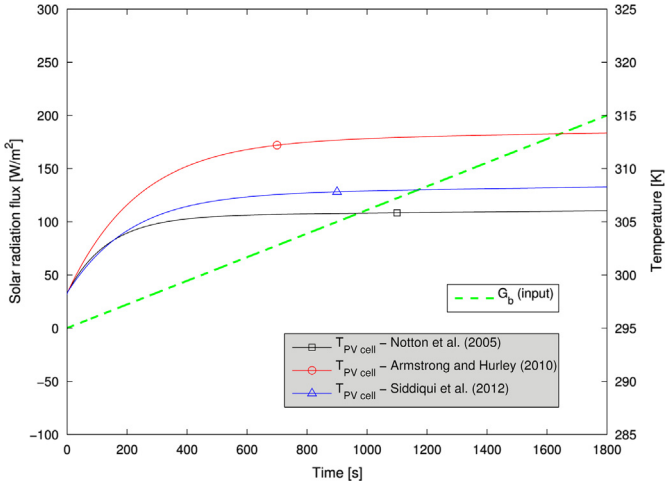

Fig. 9. PV cell temperatures with changing beam solar radiation.

sensitivity analysis represents the simplest way to understand what happens with every set of thermal boundary conditions.

4.1.1. Parametric study on PV cell temperatures

The effects of different meteorological inputs are now evaluated in four different cases. In each case, one of the inputs is assumed to linearly change according to the values found in the data measured in Ajaccio. The time of the simulation is kept to 30 min. The cases of the parametric study are summarized in Table 3.

The results of changing the ambient temperature (case 1) are shown in Fig. 7. As it can be observed in Fig. 7, the same above-mentioned tendency of the models is maintained for this specific set of inputs. The boundary conditions used by Armstrong and Hurley [2] result in the highest temperatures for the PV cells while the boundary conditions of Notton et al. [6] give the lowest temperatures. One important thing to note is the direct relationship of the ambient temperature with the PV cell temperature, both increase with nearly the same slope in the three cases.

The results of changing the global solar radiation flux (case 2) are shown in Fig. 8. This figure illustrates the same tendency in comparison with the case 1. The temperature of the cells again shows a direct relationship with the global solar radiation at which the module is exposed. A perceptible difference is the slope of the curves between the two cases, being steeper in the case 1,

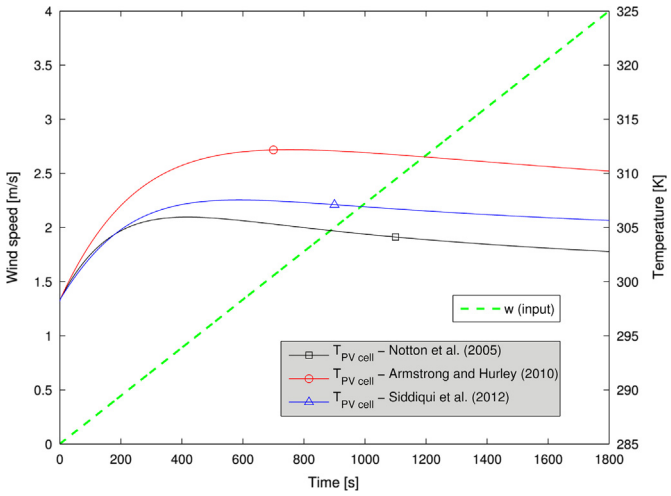

Fig. 10. PV cell temperatures with changing wind speed.

which indicates that the effect of changing the ambient temperature by 20 °C is higher that changing the global radiation by 400 W/m^2.

The PV cell temperatures of the case 3 are shown in Fig. 9. This shows the temperatures while only the beam normal solar radiation is varied. The results are very similar to those observed in the case 2 but, in this occasion, the radiation was only changed by 200 W/m^2. It is difficult to determine if the beam solar radiation has a higher or lower influence than the global radiation on the calculated temperatures, since they are always linked but they do not always have the same magnitude of proportionality. What can be said is that both components of radiation are important and both always should be measured and considered as inputs for any thermal model of this type.

The outputs obtained after running the model with a changing wind speed are shown in Fig. 10. This figure shows one peculiarity: the temperatures in the cells decrease after reaching a specific wind velocity, near or above 1 m/s. The curves in Fig. 10 show the beneficial impact of the wind over the temperatures in the PV cells, which is decreased at a similar rate. The position of the curves as a function of the assumptions used is the same as in all the previous cases, confirming the energy balance observed in the NOCT evaluation, but here in transient studies and even when the wind speed is the only parameter varied (up to 4 m/s). It is important to mention that the wind speed, main parameter in the case 4, is the key parameter in the convection coefficient calculation.

4.1.2. Parametric study on additional parameters

After seeing the results of the four cases tested previously, it is evident that the different formulations have a consistent behavior. The question at this point is: Why one set of assumptions results in a higher or lower temperature than the other? Or, in other words: What are the factors that influence the difference of the results? To answer these questions a deeper revision of some important parameters is performed using the conditions of the cases 1 and 4, which were are the most sensitive in the previous parametric study. The parameters chosen are those relevantly arising from the equations used in each thermal model, including the sky temperature, the convection heat exchange coefficients and the internal heat generation in the front glass. Wind speed is also a key parameter but was already sufficiently investigated in the previous parametric study.

As mentioned previously, the sky temperature formulation applied is different for the thermal models studied. Armstrong and Hurley [2] did not specify the equation used, leading to assume it

equal to the ambient temperature in the current study. The sky temperatures calculated for the case 1 conditions are shown in Fig. 11.

Fig. 11 shows the difference of the formulations used to calculate the sky temperature. The red line represents the sky temperature assumed for the Armstrong and Hurley [2] equations, which is in fact the ambient temperature. The other two cases, Notton et al. [6] and Siddiqui et al. [4], produce lower sky temperatures, which increase the temperature difference between the module surface and the sky and increasing the heat exchanged or released. Fig. 11 shows one of the reasons why the model used by Armstrong and Hurley [2] provides always the highest temperatures.

The convection film coefficient is the parameter that represents the major difference between the studied thermal boundary conditions, not only because each model uses a different set of equations, but also because the forced and free components are taken differently according to the side of the panel. The analysis of this parameter requires looking at the front and rear surfaces independently, based on the assumed boundary conditions. The second requirement is to observe the behavior while the temperature and the wind speed change.

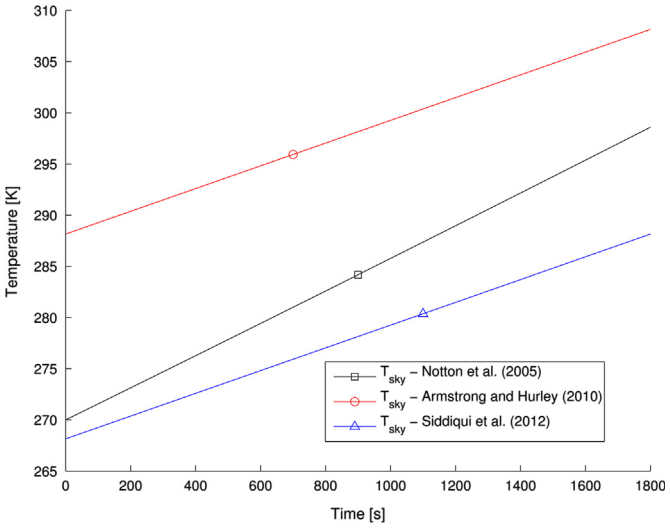

Fig. 11. Sky temperature with changing ambient temperature.

The results of the convection coefficient on the front surface are shown in Fig. 12. The plots given in this figure show the behavior of the convection coefficient while the ambient temperature and the wind speed are varied. In both cases, the boundary conditions used by Notton et al. [6] give the parameter with the highest value, allowing a higher heat exchange with or without wind and essential to keep the temperatures low inside the module. The other two curves have a similar behavior, with lower values for the equations used by Siddiqui et al. [4]. The same results for the rear surface are also shown in Fig. 13.

Fig. 13 shows the same results for the case of the Notton et al. [6] formulation, which makes sense since the same forced convection equation is used for both surfaces and the model assumes no difference with respect to the wind effect. The change in this case occurs with the blue and red solid curves: the formulations used by Siddiqui et al. [4] produce now a higher convective coefficient and the difference with the Armstrong and Hurley [2] formulation increases with the wind speed. The reason of this difference is that Armstrong and Hurley [2] only assume free convective heat exchange at the back surface, while Siddiqui et al. [4] also account for the forced part.

The next analysis is performed to see the difference in temperature in the front glass. The reason of performing such analysis is because Notton et al. [6] take into account the heat generated in the glass due to its absorptivity. The parameter reviewed is the temperature corresponding to the node located at the middle of the front glass. The results are presented in Fig. 14. The profiles of the curves show a temperature of the front glass very similar to the one observed in the PV cells. Even when we accounts for the heat generated inside the glass, the temperatures shown do not have a different behavior with respect to the previous ones. The heat generated in the glass seems to have a low influence on the temperature of the module, which is reasonable since the absorptivity of the front glass is taken to be 5% and in this kind of systems it is always desired to transmit all the energy to the cells.

4.2. Electrical model

The *I–V* curve provides basically the electrical performance of the module, showing the range of current and voltage available for the load connected to the panel at any given moment. The curve is obtained from modified one-diode models, which require a previous calculation of parameters like the series (R_s) and shunt (R_{sh}) resistances. Such resistances are computed with an optimization

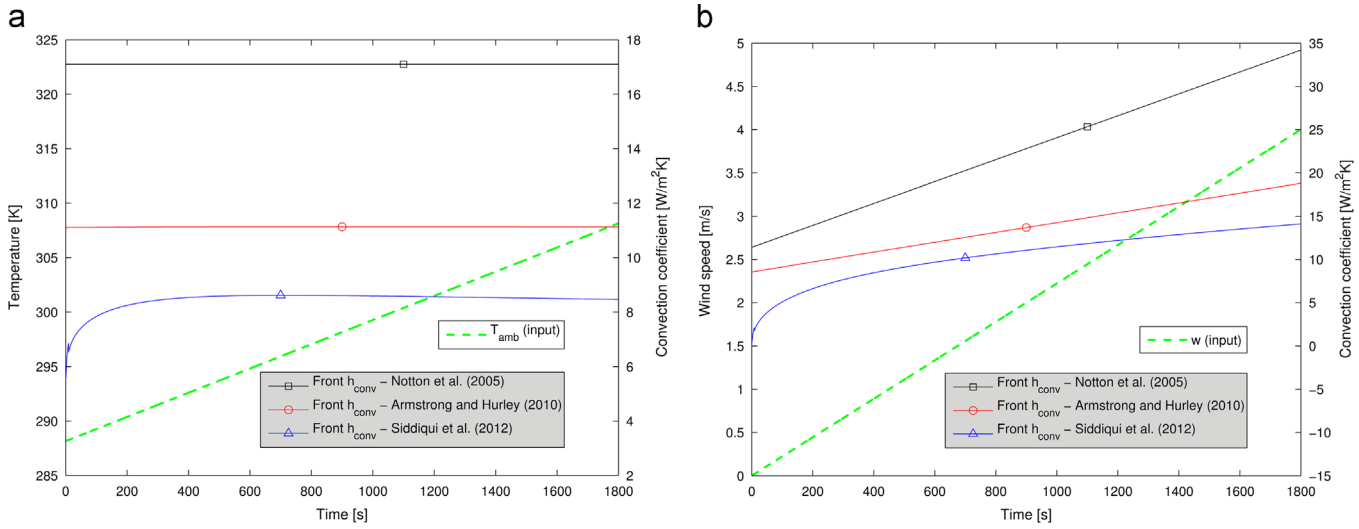

Fig. 12. Front convection coefficient with: (a) changing ambient temperature and (b) changing wind speed.

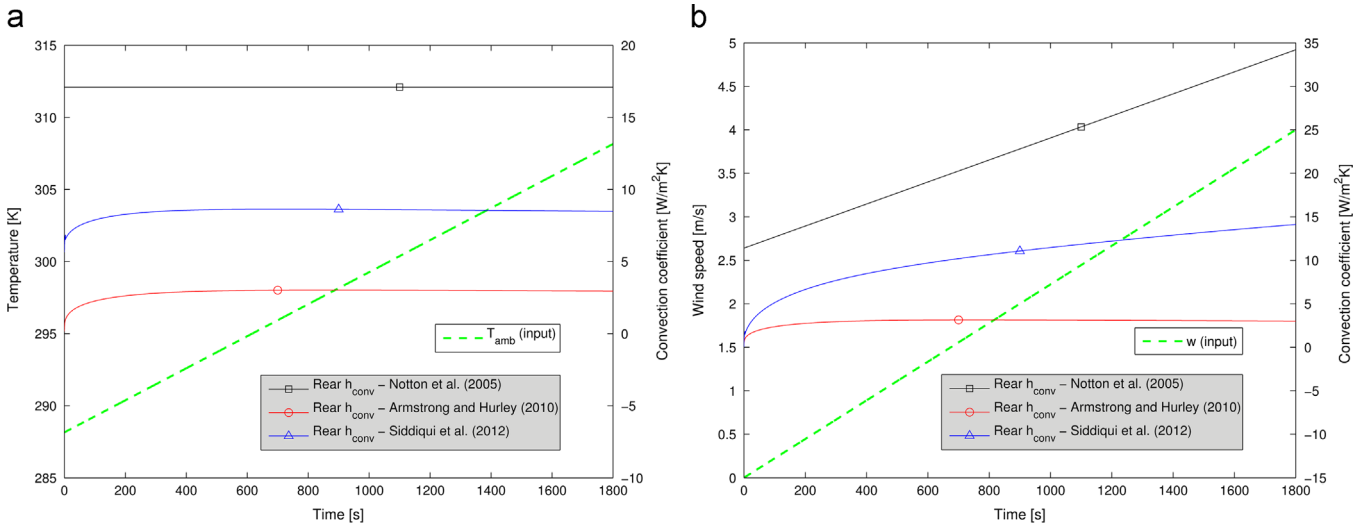

Fig. 13. Rear convection coefficient with: (a) changing ambient temperature and (b) changing wind speed.

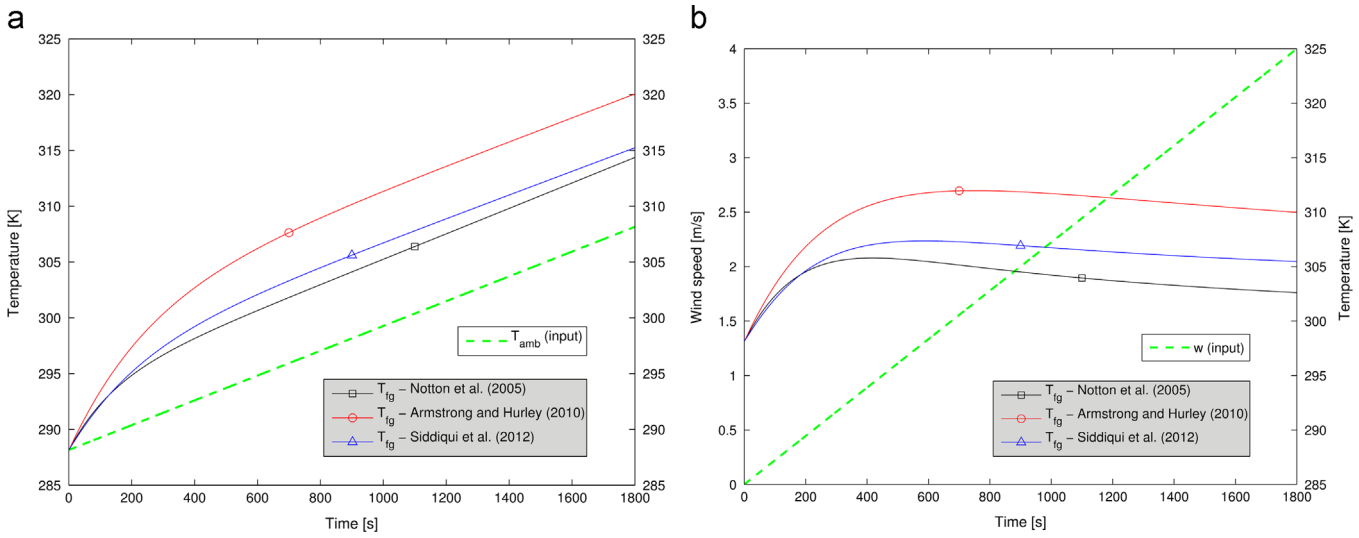

Fig. 14. Front glass temperature with: (a) changing ambient temperature, (b) changing wind speed.

Table 4
Resistances for the PV panel BP 350 obtained with the PSO algorithm at the PV cell level.

One-diode model	R_s [Ω]	R_{sh} [Ω]
Siddiqui et al. [4], Eq. (36)	0.0270	8.1217
Tsai [13], Eq. (38)	0.0277	15.0698

method based on the PSO algorithm (details on the method and its implementation in MATLAB® can be found in Sánchez Barroso et al. [14]). The results found for the series and shunt resistances applied to the models given in Eqs. (36) and (38) are shown in Table 4. Note that the ideality factor for polycrystalline silicon solar cells is assumed $A=1.025$ (Tsai [13]).

Once the values of the series and shunt resistances have been calculated, the *I–V* curve of the PV panel can be plotted. The *I–V* and *P–V* curves predicted for the PV panel BP 350 at Standard Test Conditions (STC) with the one-diode models presented by Siddiqui et al. [4] and Tsai [13] and the resistances calculated with the PSO algorithm are presented in Fig. 15.

The *I–V* and power curves can also be obtained for different operating points, namely with PV cell temperatures and solar radiations different from the ones at STC. The only requirement is to apply the translating equations to calculate the corrected parameters at the desired condition. The parameters to translate are the band gap energy E_g, the modified diode ideality factor a, the photocurrent I_L, the diode reverse saturation current I_0 and the shunt resistance R_{sh}; the series resistance R_s is assumed constant for any condition. The equations to translate the parameters are included in the work of Siddiqui et al. [34]. The curves for three different temperatures at constant solar irradiance are shown in Fig. 16a. The points included in the *I–V* curve of Fig. 16a correspond to reference points extracted from the datasheet curve. The behavior of the curves is as expected since the *I–V* curves approach very closely to the reference points. The curves for three different global solar radiations at constant cell temperature are shown in Fig. 16b. From Figs. 15 and 16, it can be said that the electrical models are then well implemented.

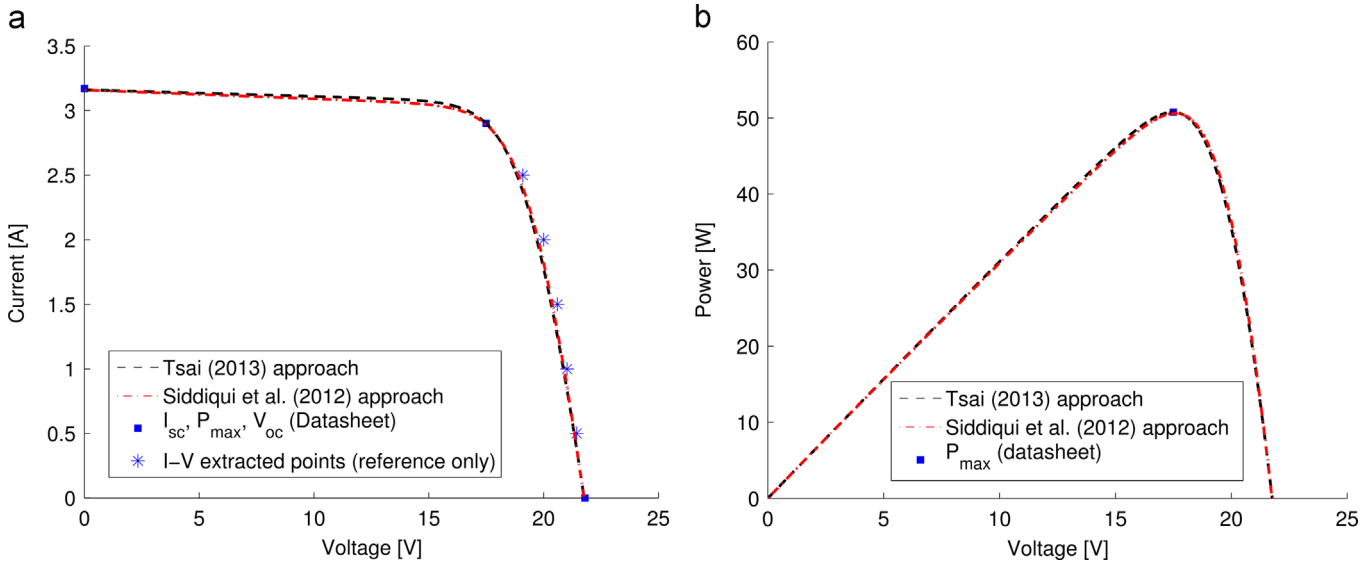

Fig. 15. Curves for the PV panel BP 350 at STC using the resistances calculated with the PSO algorithm and the modified one-diode models presented by Siddiqui et al. [4] and Tsai [13]: (a) *I–V* curves, (b) *P–V* curves.

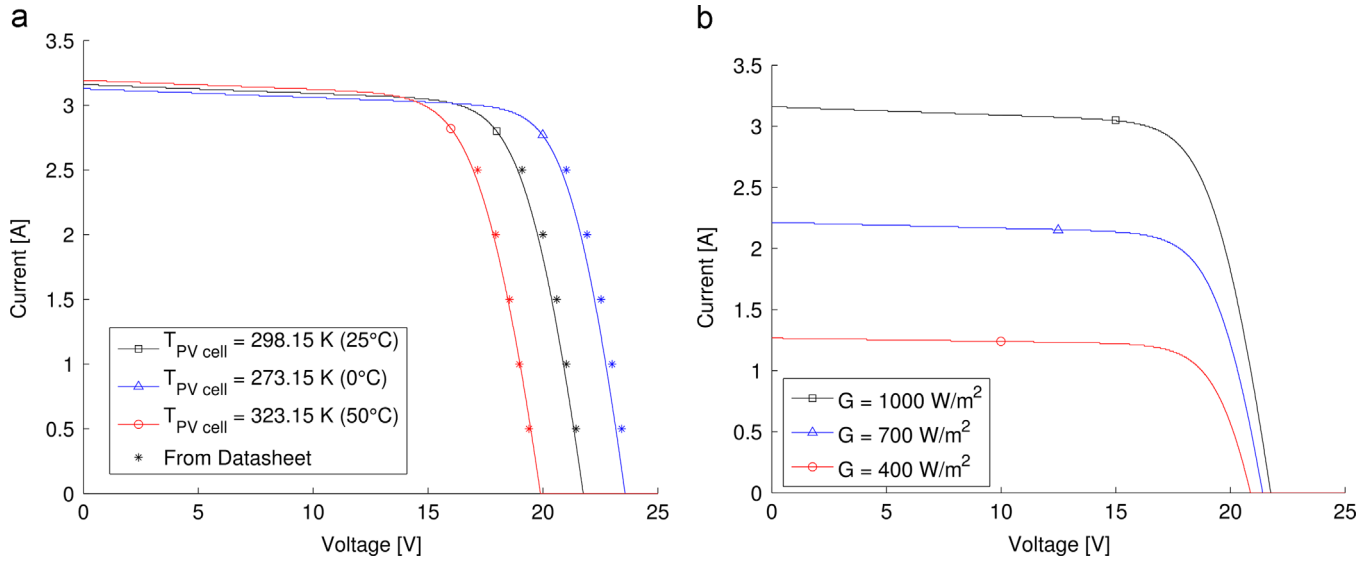

Fig. 16. Panel BP 350 *I–V* curves predicted at: (a) different cell temperatures and (b) different global solar radiations.

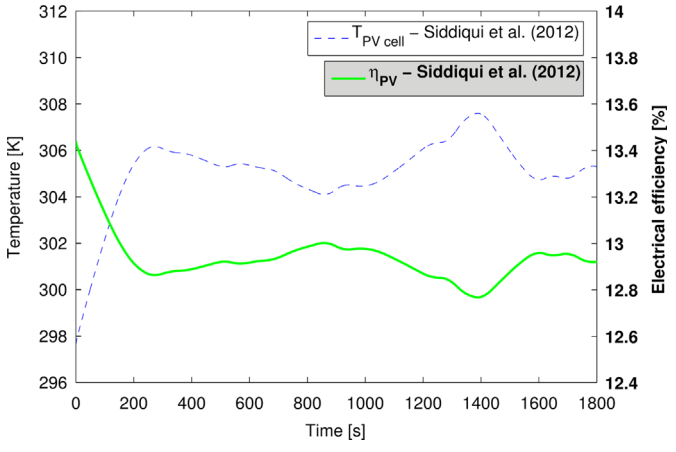

Fig. 17. Evolution of the electrical efficiency predicted with Eq.(13).

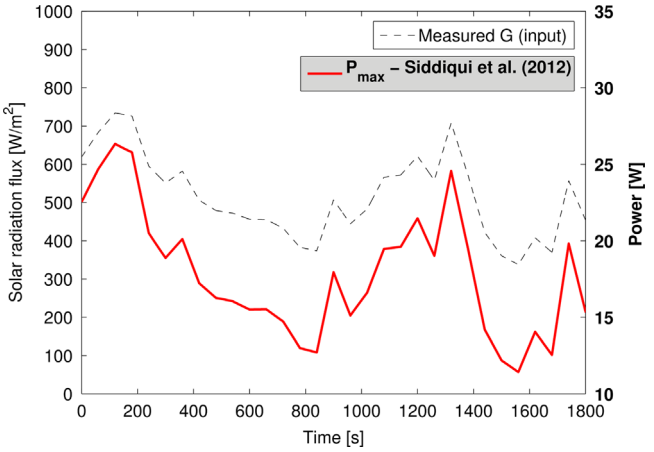

Fig. 18. Evolution of the maximum power predicted.

4.3. Evolution of efficiency and power

The efficiency and power are two of the most important parameters in the photovoltaic industry, since they account for the quality of the module and they are the base to determine whether a specific PV panel is competitive or not for a given application. These two parameters have a direct link between each other and, as stated before, they are strongly dependent on the temperature of the PV cell and the solar radiation. The evolution of the efficiency and the instantaneous power produced with the inputs provided by Professor G. Notton, and measured in Ajaccio, are shown in Figs. 17 and 18. The boundary condition assumptions applied this time are those followed by Siddiqui et al. [4] since they resulted in intermediate temperatures. The electrical efficiency as a function of time is given in Fig. 17.

As presented in Fig. 17, the electrical efficiency has a direct and opposite relationship with the PV cell temperature. When the temperature in the cell increases the efficiency decreases and vice versa. It is important to note that even when the temperature varies about 10 degrees the power efficiency coefficient changes around 0.6%. This variation is caused by the temperature coefficient provided by the PV manufacturer. In the case of the panel BP 350 the temperature coefficient used is $\beta_{Ref}=0.5\%/^{\circ}C$. The produced instantaneous power, calculated from the electrical efficiency and the measured global radiation, is plotted in Fig. 18.

The first thing to note in Fig. 18 is the correlation between the power produced and the measured radiation, clearly shown by the shape of the curves. The second thing is the amount of variation in the power produced over this period of time; the power varies from a minimum of about 12 W to a maximum of about 26 W, even when the electrical efficiency remains almost constant around 13%. The behavior of the power in comparison with the efficiency clearly suggests that even if it is important to keep a high efficiency in the cells, the energy produced will always depend on the atmospheric conditions, which are continuously changing. Fig. 18 also shows a very important aspect: the maximum power generated under real atmospheric conditions. In this case the maximum power observed is about 26 W, almost half of the power indicated in the datasheet (50 W). These numbers show the importance of having a model to predict the capabilities of a PV panel; without the thermal model it would not be possible to know that in Ajaccio, at the considered specific time, only half of the specified energy is most available.

5. Conclusions

A one-dimensional finite difference model was built and implemented in MATLAB® to calculate the temperatures inside the PV panel BP 350 while it is subjected to different atmospheric conditions. The model takes into account the formulations used by three thermal boundary conditions found in the literature, presented by Notton et al. [6], Armstrong and Hurley [2] and Siddiqui et al. [4]. The results of the different formulations were analyzed using the NOCT conditions, meteorological data from Ajaccio and a parametric study that incorporated variations in the ambient temperature, the global and beam solar radiations and the wind speed. The results of the different studies were consistent, showing that the boundary conditions used by Armstrong and Hurley [2] produced the highest temperatures in the PV cells, while the set of equations used by Notton et al. [6] gave the lowest ones. Such behavior is explained by the observations made from the parametric study, listed below:

- The sky temperature of Armstrong and Hurley [2], not specified and assumed here equal to the ambient temperature, is always higher than the other two cases, producing a lower thermal gradient between the sky and the surfaces of the panel, decreasing hence the amount of heat released by radiation.
- The convection equation chosen by Notton et al. [6] for the front and rear surfaces resulted in the highest convective coefficient for conditions with changing ambient temperature and wind speed. With such a high coefficient, the model is able to release heat by convection even with low wind conditions.
- The assumption of Armstrong and Hurley [2] for calculating only the free convective heat exchange for the rear surface produces a low convection coefficient, and its difference with the coefficient calculated by Siddiqui et al. [4] is increased with high wind conditions. Such low coefficient limits the heat released by convection, contributing to keep a high temperature inside the module.
- The heat generated in the front glass and taken into account by Notton et al. [6] does not contribute significantly to elevate the temperatures in the PV cells, which may be the reason why it is not considered by Armstrong and Hurley [2] and Siddiqui et al. [4]. The poor contribution of the glass is due to its low absorptivity, taken in this study as 5%.

The electrical performance of the PV panel was also studied. The analysis consisted in implementing two different one-diode models found in the literature, proposed by Siddiqui et al. [4] and Tsai [13]. Both models, capable of working for any PV panel, required the calculation of two important parameters hardly found in the literature, the series and shunt resistances. One optimization method based on the movement of swarms was implemented to calculate such resistances, named PSO algorithm. After obtaining the resistances, the considered one-diode models were tested with standard test conditions and compared against the data found in the module datasheet. Both models gave acceptable and similar results for the *I–V* response even when the calculated resistances were considerably different.

The evolution of the electrical efficiency showed in general a small variation to the continuously changing ambient conditions, explained mainly by the low temperature coefficient given by the PV manufacturer. The maximum power produced, on the contrary, showed a high variation in time, affected mostly by the solar radiation. The calculated power showed to be considerably low in comparison with the rated power given in the datasheet, which proves the relevance of the predictive approaches studied in this article.

Acknowledgments

The authors would like to thank Professor G. Notton, from the University of Corsica, for providing us with experimental data from Ajaccio. One of the authors, Sánchez Barroso, would like to thank the Mexican National Council for Science and Technology CONACYT for providing him with assistantship. We also thank Dr. Sabre Kais from QEERI–Qatar Foundation, for providing support to J.C. Sánchez Barroso during a visit with QEERI.

References

[1] T.M. Razykov, C.S. Ferekides, D. Morel, E. Stefanakos, H.S. Ullal, H. M. Upadhyaya, Solar photovoltaic electricity: Current status and future prospects, Sol. Energy 85 (2011) 1580–1608, http://dx.doi.org/10.1016/j.solener.2010.12.002.

[2] S. Armstrong, W.G. Hurley, A thermal model for photovoltaic panels under varying atmospheric conditions, Appl. Therm. Eng. 30 (2010) 1488–1495, http://dx.doi.org/10.1016/j.applthermaleng.2010.03.012.

[3] E. Skoplaki, J.A. Palyvos, On the temperature dependence of photovoltaic module electrical performance: a review of efficiency/power correlations, Sol. Energy 83 (2009) 614–624, http://dx.doi.org/10.1016/j.solener.2008.10.008.
[4] M.U. Siddiqui, A.F.M. Arif, L. Kelley, S. Dubowsky, Three-dimensional thermal modeling of a photovoltaic module under varying conditions, Sol. Energy 86 (2012) 2620–2631, http://dx.doi.org/10.1016/j.solener.2012.05.034.
[5] A.D. Jones, C.P. Underwood, A thermal model for photovoltaic systems, Sol. Energy 70 (2001) 349–359, http://dx.doi.org/10.1016/S0038-092X(00)00149-3.
[6] G. Notton, C. Cristofari, M. Mattei, P. Poggi, Modelling of a double-glass photovoltaic module using finite differences, Appl. Therm. Eng. 25 (2005) 2854–2877, http://dx.doi.org/10.1016/j.applthermaleng.2005.02.008.
[7] V. Lo Brano, G. Ciulla, A. Piacentino, F. Cardona, Finite difference thermal model of a latent heat storage system coupled with a photovoltaic device: description and experimental validation, Renew. Energy 68 (2014) 181–193, http://dx.doi.org/10.1016/j.renene.2014.01.043.
[8] I. Caluianu, F. Bălțăreţu, Thermal modelling of a photovoltaic module under variable free convection conditions, Appl. Therm. Eng. 33–34 (2012) 86–91, http://dx.doi.org/10.1016/j.applthermaleng.2011.09.016.
[9] O. Hasan, A.F.M. Arif, Performance and life prediction model for photovoltaic modules: Effect of encapsulant constitutive behavior, Sol. Energy Mater. Sol. Cells 122 (2014) 75–87, http://dx.doi.org/10.1016/j.solmat.2013.11.016.
[10] E. Sartori, Comments on "A thermal model for PV panels under varying atmospheric conditions", by S. Armstrong and W.G. Hurley, Applied Thermal Engineering 30 (2010) 1488–1495, Appl. Therm. Eng. 31 (2011) 400, http://dx.doi.org/10.1016/j.applthermaleng.2010.08.006.
[11] S. Armstrong, W.G. Hurley, Response to comments by E. Sartori on "A thermal model for PV panels under varying atmospheric conditions", by S. Armstrong and W.G. Hurley, Applied Thermal Engineering 30, Appl. Therm. Eng. 31 (2011) 1488–1495, http://dx.doi.org/10.1016/j.applthermaleng.2010.08.005.
[12] S. Kumar Natarajan, M. Katz, T. Kumar Mallick, Thermal model for an early prototype of concentrating photovoltaic for active solar panel initiative system, J. Renew. Sustain. Energy 4 (2012) 011601-1–011601-7, http://dx.doi.org/10.1063/1.3683513.
[13] H. Tsai, Complete PV model considering its thermal dynamics, J. Chin. Inst. Eng. 36 (2013) 1073–1082, http://dx.doi.org/10.1080/02533839.2012.747044.
[14] J.C. Sanchez Barroso, J.P.M. Correia, N. Barth, S. Ahzi, M.A. Khaleel, A PSO algorithm for the calculation of the series and shunt resistances of the PV panel one-diode model, in: Proceedings of the 2014 International Renewable and Sustainable Energy Conference (IRSEC), 2014, pp. 1–6. http://dx.doi.org/10.1109/IRSEC.2014.7059883.
[15] J.A. Duffie, W.A. Beckman, Solar Engineering of Thermal Processes, fourth ed., John Wiley & Sons, Inc,, Hoboken, New Jersey, U.S.A, 2013.
[16] R.J. Cole, N.S. Sturrock, The convective heat exchange at the external surface of buildings, Build. Environ. 12 (1977) 207–214, http://dx.doi.org/10.1016/0360-1323(77)90021-X.
[17] F.L. Test, R.C. Lessmann, A. Johary, Heat transfer during wind flow over rectangular bodies in the natural environment, J. Heat Transf. 103 (1981) 262–267, http://dx.doi.org/10.1115/1.3244451.
[18] A. Bejan, A.D. Kraus, Heat Transfer Handbook, Wiley, Hoboken, New Jersey, U.S.A, 2003.
[19] F.P. Incropera, D.P. DeWitt, Fundamentals of Heat and Mass Transfer, John Wiley & Sons, Inc, Hoboken, New Jersey, U.S.A, 2002.
[20] E.M. Sparrow, J.W. Ramsey, E.A. Mass, Effect of finite width on heat transfer and fluid flow about an inclined rectangular plate, J. Heat Transf. 101 (1979) 199–204, http://dx.doi.org/10.1115/1.3450946.
[21] J.R. Lloyd, W.R. Moran, Natural convection adjacent to horizontal surface of various planforms, J. Heat Transf. 96 (1974) 443–447, http://dx.doi.org/10.1115/1.3450224.
[22] W.C. Swinbank, Long-wave radiation from clear skies, Q. J. R. Meteorol. Soc. 89 (1963) 339–348, http://dx.doi.org/10.1002/qj.49708938105.
[23] B. Alsayid, Modeling and simulation of photovoltaic cell/module/array with two-diode model, Int. J. Comput. Technol. Electron. Eng. 2 (2012) 6–11.
[24] H. Matsukawa, K. Kurokawa, Temperature fluctuation analysis of photovoltaic modules at short time interval, Conference Record of the Thirty-first IEEE, 2005, pp. 1816–1819. http://dx.doi.org/10.1109/PVSC.2005.1488505.
[25] Z.H. Lu, Q. Yao, Energy analysis of silicon solar cell modules based on an optical model for arbitrary layers, Sol. Energy 81 (2007) 636–647, http://dx.doi.org/10.1016/j.solener.2006.08.014.
[26] W. Jooß, Multicrystalline and Back Contact Buried Contact Silicon Solar Cells, Fachbereich Physik, Universität Konstanz, Germany, 2002, Ph.D. dissertation.
[27] J. Lai, T. Perazzo, Z. Shi, A. Majumdar, Optimization and performance of high-resolution micro-optomechanical thermal sensors, Sens. Actuators A 58 (1997) 113–119, http://dx.doi.org/10.1016/S0924-4247(96)01401-X.
[28] G.J.M. Phylipsen, E.A. Alsema, Environmental Life-Cycle Assessment of Multicrystalline Silicon Solar Cell Modules, Netherlands Agency for Energy and the Environment, 1995, Report No. 95057, Department of Science, Technology and Society, Utrecht University, Padualaan 14, NL-3584 CH Utrecht, The Netherlands.
[29] J.E. Hatsch, Aluminum: Properties and Physical Metallurgy, second ed., ASM International, Metals Park, Ohio, U.S.A, 1984.
[30] M.D. Bazilian, H. Kamalanathan, D.K. Prasad, Thermographic analysis of a building integrated photovoltaic system, Renew. Energy 26 (2002) 449–461, http://dx.doi.org/10.1016/S0960-1481(01)00142-2.
[31] ABAQUS FEA, Theory Manual Section 2.11.1, 2012.
[32] N. Barth, D. George, S. Ahzi, Y. Rémond, V. Doquet, F. Bouyer, S. Bétremieux, Modeling and simulation of the cooling process of borosilicate glass, J. Eng. Mater. Technol. 134 (2012) 041001-1–041001-10, http://dx.doi.org/10.1115/1.4006132.
[33] N. Barth, J.P.M. Correia, S. Ahzi, M.A. Khaleel, Thermal analysis of solar panels, TMS – Middle East – Mediterranean Materials Congress (MEMA 2015) (2015) 441-450. http://dx.doi.org/10.1002/9781119090427.ch47.
[34] M.U. Siddiqui, A.F.M. Arif, A.M. Bilton, S. Dubowsky, M. Elshafei, An improved electric circuit model for photovoltaic modules based on sensitivity analysis, Sol. Energy 90 (2013) 29–42, http://dx.doi.org/10.1016/j.solener.2012.12.021.